Reaction Kinetics and Reactor Modeling of the Plasma Etching of Silicon

A model including the effects of diffusion and convection can be used to predict the etch rate of crystalline silicon in a plasma discharge of nitrogen trifluoride. The case of a radial flow reactor with crystalline silicon wafers located at discrete positions can be solved using a finite-element solution to a boundary value problem. Such a model is useful to predict the effects of pressure, flow rate of etchant gas, percent silicon exposed, and wafer position on both inter- and intrawafer etch rates. It was found from modeling that greater uniformity in etch rate is achieved by lowering the pressure and percent exposure of silicon, and to a lesser degree the volumetric flow rate.

H. G. Stenger, Jr., H. S. Caram, and C. F. Sullivan
Department of Chemical Engineering
Lehigh University
Bethlehem, PA 18015

W. M. Russo
IBM Corporation
General Technology Division
Essex Junction, VT 05452

Introduction

Etching is the process of selectively removing material to define features such as lines, holes, or trenches in semiconductor materials. In plasma etching a glow discharge is used to generate highly reactive etching species from relatively inert gases. The discharge is maintained between two electrodes with one electrode driven with an oscillating voltage and the other electrode held at ground. Energetic electrons driven by the electrodes react with neutral molecules to form active free radicals and positive ions. The voltage oscillations between the electrodes result in long electron lifetimes, thus increasing their reactivity. Masked semiconductor wafers are placed either on the driven or the grounded electrode. For commercial reactors the shapes of the electrodes include concentric cylinders, barrel-shaped polyhedra, symmetric parallel plates, and unsymmetric parallel plates. The reactor sizes are large enough to hold up to eighteen 125 mm wafers, or are as small as just one wafer. Pressures are low, typically less than 1 torr (133 Pa) and as low as 10 millitorr (1.33 Pa) for special applications of reactive ion etching (Bollinger et al., 1984). Reviews of reactor technology are given by Fonash (1985) and Mathad (1985), and of plasma physics by Sawin (1985).

The number of etching gas-solid combinations is large (Flamm et al., 1984). However in almost all cases the etchant product is a volatile halogen compound of the etched solid. For silicon etching, NF_3 (Bower, 1982; Ianno et al., 1981; Woytek et al., 1984), SF_6 (Eisele, 1981), and CF_4 (Flamm, 1979) have all been shown to be good etchants. For etching aluminum or aluminum-copper, CCl_4 (Tokunaga and Hess, 1980), Cl_2 and/or BCl_3 (Hess, 1982) are commonly used. Molybdenum and tungsten silicides are etched rapidly with NF_3 (Korman et al., 1983) and CF_4/O_2 (Chow and Steckl, 1984). Hydrogen is added to the fluorinated compounds to enhance the etch selectivity of silicon dioxide over silicon (Ephrath, 1979), while oxygen can be added to prevent the deposition of polymeric residue when etching with CF_4 or SF_6 (Mogab et al., 1978). In the present work, NF_3 etching of Si is examined specifically, however much of the kinetic modeling is generic and can be applied to other etching systems.

Common to all etching systems are two major processing difficulties: etch *anisotropy* (or the ability to produce clean vertical walls when etching) and etch rate *uniformity* from wafer to wafer (interwafer) and within a single wafer (intrawafer). Determining the causes of isotropic etching and nonuniformity requires an accurate understanding of the chemical and physical reactions occurring as well as an accurate model of the reactor's fluid dynamics. Attempts have been made to quantify the influence of reactor geometry on etch rate (Battey, 1977; Mogab, 1977; Winters et al., 1978; Zarowin, 1984, 1985; Alkire and Economou, 1985; Jensen et al., 1986), however only a few *predictive* models exist that are useful for correcting nonuniformity and isotropy problems. For example, Alkire and Economou show the importance of wafer spacing when stripping photoresist in a barrel reactor, however they do not extend their work to the etching of semiconductor materials in parallel-electrode systems. Jensen et al. do consider the problem of a parallel-electrode system for etching silicon with CF_4/O_2. In their analysis they present the solution of the etch rate in a reactor containing a uniform and symmetric loading of silicon in the reactor. Since in practice silicon wafers are discrete sources of silicon the geometry assumed in their work is not complete.

In previous work (Stenger and Akiki, 1986), our group has developed the chemical kinetic parameters needed to predict etch rate. In the present work we use those parameters to model a radial flow plasma reactor with various wafer locations, loadings, and process conditions.

Experimental Method

The reactor chosen for the present work has a parallel plate radial flow configuration and is loaded with silicon wafers at discrete locations. The radial flow configuration is widely used, although it is known to exhibit nonuniform etch rates from wafer to wafer and across a single wafer. The etchant gas chosen for this work is nitrogen trifluoride diluted in argon. Etching of amorphous and crystalline silicon in a nitrogen trifluoride plasma discharge has been shown to possess several practical advantages over fluorocarbon gas discharges (Ianno et al., 1981). Rapid etch rates and high etch selectivity are the primary advantages of NF_3 plasma etching (Woytek et al., 1984). In addition, NF_3 has the advantage of producing entirely gaseous etch products, while fluorocarbon etchants are known to form polymer deposits during etching, a complication that Jensen et al. (1986) omit in their model. However, the NF_3 etching mechanism has the disadvantage of being controlled by neutral free radicals, while results in more isotropic (nonvertical wall) etch profiles (Bower, 1982).

Experimental measurements were made in the PlasmaTherm PK-24 radial flow reactor shown in Figure 1. The electrode spacing was 1.57 cm and the diameter of both the upper and lower electrodes was 55.9 cm. These dimensions give an electrode area of 2,450 cm^2 and a reactor volume of 3,850 cm^3. Both electrodes were made of stainless steel and had imbedded coils for cooling water circulation. The upper electrode was connected through a capacitive tuner to a 3 kW radio frequency (13.56 MHz) power supply, while the lower electrode was grounded.

Nitrogen trifluoride (Air Products and Chemicals, Inc.) and argon (Union Carbide Co., Linde Division) were fed separately

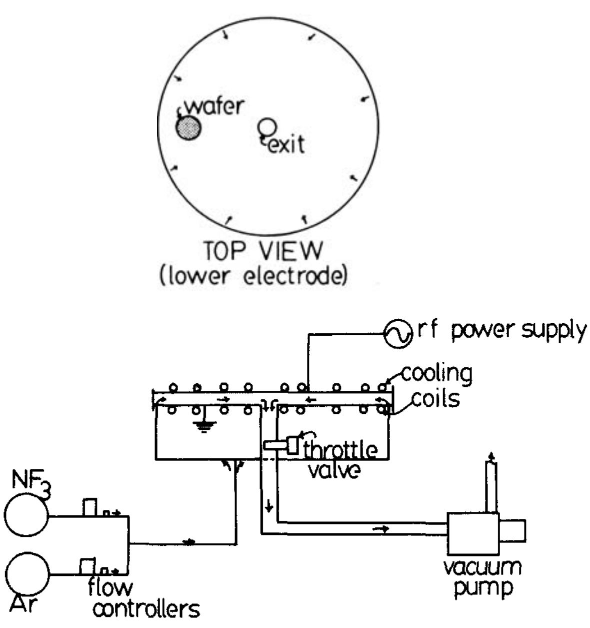

Figure 1. Experimental apparatus used for plasma etching.

through individual mass flow controllers (Vacuum General, Inc.) and mixed upstream of the reactor. The gases entered the reactor through a 1/4 in. (6.4 mm) perforated tube located at the outer perimeter of the lower electrode. Pressure was controlled with an electrically actuated throttle valve located between the reactor chamber and vacuum pump (Alcatel, Inc. model 2600).

The etching material used was single crystal silicon (Virginia Semiconductor) with the ⟨100⟩ face exposed to the etching gases. The wafers were placed on the lower electrode and etch time was typically 30 min. Etch rates were measured as the weight loss of the wafer divided by the run time. Varying the run time from 10 to 45 min gave similar etch rates, indicating that etch rate was independent of etch time.

Theory

Chemical kinetics

It is generally accepted that plasma etching of silicon with fluorinated compounds proceeds through the formation of volatile SiF_2 and SiF_4 (Flamm et al., 1984). Although the number of possible reactions is large, the overall etching phenomena can be represented by a smaller subset of reactions, composed of those reactions that are the most probable and that are necessary to explain the observed results.

The first necessary and probable reaction is the dissociation by electron bombardment of NF_3 to form free radical fluorine and a combination of NF_2, NF, and N_2.

$$NF_3 + e- \xrightarrow{k_1} NF_{3-x} + xF + e- \tag{1}$$

This reaction has been reported by Greenberg and Verdeyen (1985) and Stenger and Akiki (1986) to be an extremely rapid reaction in a plasma discharge. The undetermined stoichiometric coefficient, x, reflects the combination of species produced (Greenberg and Verdeyen).

Measurements by Flamm et al. (1981) have shown that over a wide range of temperature and atomic fluorine concentration, the removal of silicon from the wafer surface is first order in fluorine concentration. Their mechanism postulates that the Si surface is rapidly saturated with fluorine and that the rate-limiting step is the chemical desportion of SiF_2:

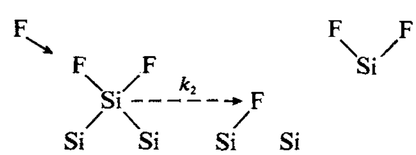

(2)

Once desorbed, SiF_2 will rapidly perfluorinate to form stable SiF_4, which is the observed end product of the etching reaction. An alternative to chemical desportion is ion-induced desorption, where an ion, driven by the potential difference between the plasma phase and the electrode (which can be several tens of electron volts), strikes the silicon surface and causes SiF_2 to desorb (Sawin and Thompson, 1986). Ion-induced desorption is known to give highly anisotropic etch profiles. From the observation that NF_3 etching is predominantly isotropic (Bower, 1982), it is assumed here that the ion-induced reaction is negligible.

Although atomic fluorine is relatively long lived at the low pressures of the discharge (<60 Pa), it has a finite probability of recombining with F or NF_x to form inactive F_2 or NF_{x+1} (Honda and Brandt, 1984) through so-called loss reactions (Mogab, 1984). In this work these reactions are assumed to be first order with respect to fluorine concentration (with a rate coefficient k_3), and to be homogeneous.

From the proposed reactions, the homogeneous and heterogeneous rate of disappearance of the species will be:

$$\text{Fluorine:}\quad r_F = -xk_1[NF_3][e-] + 4k_2 a_{Si} + k_3[F] \tag{3}$$

$$NF_3:\quad r_{NF_3} = k_1[NF_3][e-] \tag{4}$$

$$\text{Silicon:}\quad r_{Si} = +k_2[F]a_{Si} \tag{5}$$

$$SiF_4:\quad r_{SiF_4} = -k_2[F]a_{Si} \tag{6}$$

In earlier work, Stenger and Akiki (1986) determined values for k_1, x, k_2, and k_3 at 25°C using mixtures of NF_3 and argon in the same PK-24 reactor. Under the assumption of a well-mixed reactor, k_1 was found to be immeasurably large, indicating that fluorine atoms are generated rapidly in a narrow region at the reactor entrance. They are then depleted due to loss and etching reactions between the reactor entrance and exit. The stoichiometric coefficient x obtained from their work was 1.83, indicating that one to two fluorine atoms are generated per molecule of NF_3 introduced into the reactor. The reaction rate constants, k_2 and k_3, were experimentally determined to be 23.5 cm/s and 0.57 s^{-1}, respectively.

Reactor modeling

Assuming steady state conditions, radial flow parallel to the electrodes ($v_z = v_\theta = 0$), and the homogeneous fluorine loss reaction to be first order on the concentration of fluorine, the concentration of fluorine atoms in the reactor is described by:

$$v_r \frac{\partial c_a}{\partial r} = \mathcal{D}\left[\frac{1}{r}\frac{\partial}{\partial r}\left(r\frac{\partial c_a}{\partial r}\right) + \frac{1}{r^2}\frac{\partial^2 c_a}{\partial \theta^2} + \frac{\partial^2 c_a}{\partial z^2}\right] - k_3 c_a \tag{7}$$

It is convenient to average the concentration equation across the thickness of the reactor, i.e.,

$$\bar{c} = \frac{1}{2h}\int_{-h}^{h} c_a\, dz \tag{8}$$

$$\frac{1}{2h}\int_{-h}^{h} v_r \frac{\partial c_a}{\partial r} dz = \frac{\mathcal{D}}{2h}\left\{\int_{-h}^{h}\left[\frac{1}{r}\frac{\partial}{\partial r}\left(r\frac{\partial c_a}{\partial r}\right) + \frac{1}{r^2}\frac{\partial^2_{c_a}}{\partial \theta^2}\right]dz + \left(\frac{\partial c_a}{\partial z}\right)_{z=h} - \left(\frac{\partial c_a}{\partial z}\right)_{z=-h}\right\} - \frac{k_3}{2h}\int_{-h}^{h} c_a\, dz \tag{9}$$

The terms $\mathcal{D}\ (\partial c_a/\partial z)_{z=\pm h}$ represent flow normal to the surface of the electrodes. There is flow only at the surface of the wafers, and we again assume the etching rate to be a first-order reaction on the concentration of fluorine atoms. This implies that

$$\mathcal{D}\left(\frac{\partial c_a}{\partial z}\right)_{z=h} = 0 \tag{10}$$

$$\mathcal{D}\left(\frac{\partial c_a}{\partial z}\right)_{z=-h} = S(r,\theta)k_2(c_a)_{z=-h} \tag{11}$$

with $S(r, \theta) = 1$ at the wafer surface and zero everywhere else. This yields

$$\frac{1}{2h}\int_{-h}^{h} v_r \frac{\partial c_a}{\partial r} dz = \frac{\mathcal{D}}{2h}\left\{\int_{-h}^{h}\left[\frac{1}{r}\frac{\partial}{\partial r}\left(r\frac{\partial c_a}{\partial r}\right) + \frac{1}{r^2}\frac{\partial^2_{c_a}}{\partial \theta^2}\right]dz\right\} - \frac{Sk_2}{2h}\bar{c} - k_3\bar{c} \tag{12}$$

As will be justified below, it is reasonable to assume that the radial and tangential derivatives of the concentration are independent of z. Under these conditions the vertical average of the fluorine concentration satisfies:

$$\frac{\partial \bar{c}}{\partial r}\frac{1}{2h}\int_{-h}^{h} v_r\, dz = \mathcal{D}\left\{\frac{1}{r}\frac{\partial}{\partial r}\left(r\frac{\partial \bar{c}}{\partial r}\right) + \frac{1}{r^2}\frac{\partial^2 \bar{c}}{\partial \theta^2}\right\}\int_{-h}^{h} dz - \frac{Sk_2}{2h}\bar{c} - k_3\bar{c}$$

that after integration gives:

$$\bar{v}_r \frac{\partial \bar{c}}{\partial r} = \mathcal{D}\left[\frac{1}{r}\frac{\partial}{\partial r}\left(r\frac{\partial \bar{c}}{\partial r}\right) + \frac{1}{r^2}\frac{\partial^2 \bar{c}}{\partial \theta^2}\right] - \frac{Sk_2}{2h}\bar{c} - k_3\bar{c} \tag{13}$$

From continuity and ignoring changes in the molar flow:

$$\frac{1}{r}\frac{\partial}{\partial r}(r\bar{v}_r) = 0 \text{ and } \bar{v}_r\, \bar{v}_0 \text{ at } r = r_0 \tag{14}$$

$$\bar{v}_r = \frac{\bar{v}_0 r_0}{r} \tag{15}$$

$$\frac{\bar{v}_0 r_0}{r}\frac{\partial \bar{c}}{\partial r} = \mathcal{D}\left[\frac{1}{r}\frac{\partial}{\partial r}\left(r\frac{\partial \bar{c}}{\partial r}\right) + \frac{1}{r^2}\frac{\partial^2 \bar{c}}{\partial \theta^2}\right] - \frac{Sk_2}{2h}\bar{c} - k_3\bar{c} \tag{16}$$

Boundary conditions need be specified only at the entrance and exit of the reactor. No obvious boundary conditions are available. At the reactor entrance, however, the sum of the convective and diffusive fluxes should be equal to the total flux of reactant entering the reactor. At the exit, we require constant reactant concentration beyond the boundaries of the reactor. This implies no diffusive flux out of the reactor. This is the reasoning that yields the Danckwerts boundary conditions:

$$\frac{\partial \bar{c}}{\partial r} = 0 \text{ at } r = r_i \tag{17}$$

$$\mathcal{D}\frac{\partial \bar{c}}{\partial r} = \bar{v}_0(\bar{c} - \bar{c}_0) \text{ at } r = r_0 \tag{18}$$

Notice that we have neglected the change in concentration in the vertical direction. This can be heuristically justified by observing that if the vertical concentration profile of fluorine is convex upward, an upper bound in the change of concentration across the thickness of the reactor is given by:

$$|\Delta c_a|_{\max} \le 2h\left(\frac{\partial c_a}{\partial z}\right)_{z=-h} = \frac{2hk_2c_a}{\mathcal{D}} \tag{19}$$

The change in concentration relative to the concentration at the wafer surface (that is in principle smaller than the concentration in the bulk of the flow) will then be a modified Biot number:

$$\frac{|\Delta c_a|_{max}}{c_a} = B_i = \frac{2hk_2}{\mathcal{D}} \tag{20}$$

For typical values of the parameters ($\mathcal{D}$ = 1,000 cm^2/s, k_2 = 24 cm/s, h = 0.75 cm) this gives B_i = 0.038 or a maximum variation of 4% in the concentration in the vertical direction. There is, then, no significant error in the use of the average vertical concentration in the computation.

The equations may be made dimensionless by means of the following definitions.

$$x = \frac{r}{r_0} \quad y = \frac{\bar{c}}{\bar{c}_0} \tag{21}$$

$$a = \frac{\bar{v}_0 r_0}{\mathcal{D}} \quad b = \frac{k_3 r_0^2}{\mathcal{D}} \quad c = \frac{k_2 r_0^2}{2h\mathcal{D}} \tag{22}$$

Finally:

$$\frac{1}{x}\frac{\partial}{\partial x}\left(x\frac{\partial y}{\partial x}\right) + \frac{1}{x^2}\frac{\partial^2 y}{\partial \theta^2} - \frac{a}{x}\frac{\partial y}{\partial x} - by - Scy = 0 \tag{23}$$

$$\frac{\partial y}{\partial x} = 0 \text{ at } x = x_i \quad \text{and} \quad \frac{\partial y}{\partial x} = a(y-1) \text{ at } x = 1 \tag{24}$$

The finite-element package TWODEPEP (IMSL, 1983) was chosen to solve this problem. It is a small, general-purpose program designed for generality, ease of use, storage efficiency, and speed. It solves elliptic, parabolic, and eigenvalue partial differential equations in general two-dimensional regions. It includes a preprocessor and a graphic output package, and can automatically refine and grade the triangular mesh.

Results

Evaluation of kinetic constants

To verify the accuracy of the kinetic constants determined under the well-mixed reactor assumption (k_2 and k_3), the data of Stenger and Akiki (1986) were reevaluated with the reactor model presented here. Fitting the etch rate data from the previous work with the dispersed flow model, k_2 and k_3 were found to be 24.8 cm/s and 0.55 s^{-1}, respectively, compared to 23.5 cm/s and 0.57 s^{-1} reported by Stenger and Akiki. This close agreement between the constants determined from each model indicates that the reactor is nearly well mixed. However even with this large amount of dispersion, it will be shown that there are significant etch rate profiles from wafer to wafer and across individual wafers.

Comparison of model with experiment

Two loading configurations were chosen to illustrate the influence of wafer location and wafer crowding on etch rate uniformity. Figure 2a diagrams the case of an in-line configuration where four 50 mm dia. wafers are placed in a line from the outer to the inner radius. The second configuration, Figure 2b, referred to as spread-out, maintains the wafers at the same radius as in Figure 2a; however, each wafer is rotated about the reactor axis 90 degrees. It is expected that this second configuration would give higher etch rates since the availability of fluorine from nonetching areas of the reactor would be greater.

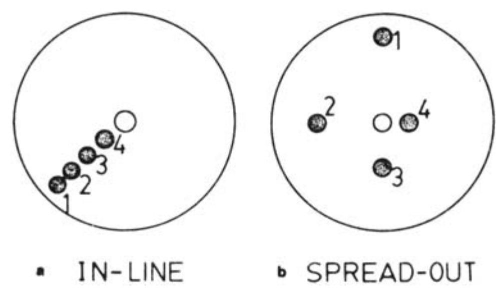

Figure 2. In-line and spread-out wafer configurations.

For the experimental runs the reactor pressure was 0.30 torr (40 Pa), the inlet mole fraction of NF_3 was 0.4, the electrode temperatures were 25°C, and the inlet flow rates were varied from 11 to 59 sccm (std cm^3/min). The dispersed-flow model was solved as outlined previously for each of the experimental conditions. The parameters used in the model solution were k_2 = 24.8 cm/s, k_3 = 0.55 s^{-1}, x = 1.83, and $\mathcal{D}$ = 680 cm^2/s (Bird et al., 1960). The solution of the model for the in-line configuration is plotted in Figure 3 together with experimentally measured etch rates for four inlet flow rates. In Figure 3 the etch rates calculated from the model are the average etch rates over the whole wafer. This allows an equivalent comparison to the experimental data, since the experimental etch rate was calculated from the weight loss of each wafer divided by the run time.

The fact that both the model and the data show a minimum in the etch rate with respect to reactor radius is particularly interesting. Since the kinetics assume that the generation of fluorine species is infinitely fast, the maximum concentration of fluorine would be expected at the reactor entrance. However the convergence of flow at the reactor center, due to the radial configuration, has the effect of increasing the concentration of fluorine by supplying F atoms from nonetching areas of the reactor.

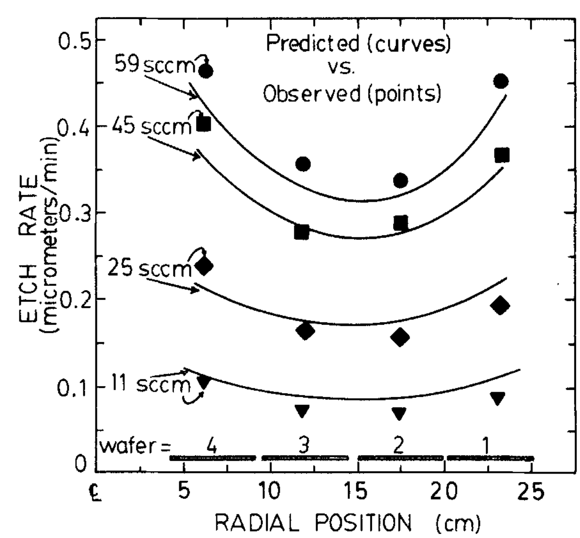

Figure 3. Predicted (curves) vs. observed (points) wafer-averaged etch rate for in-line configuration.
Temp., 25°C; press., 40 Pa; inlet NF_3 mol frac., 0.4
Inlet flow rates in std cm^3/min (sccm)

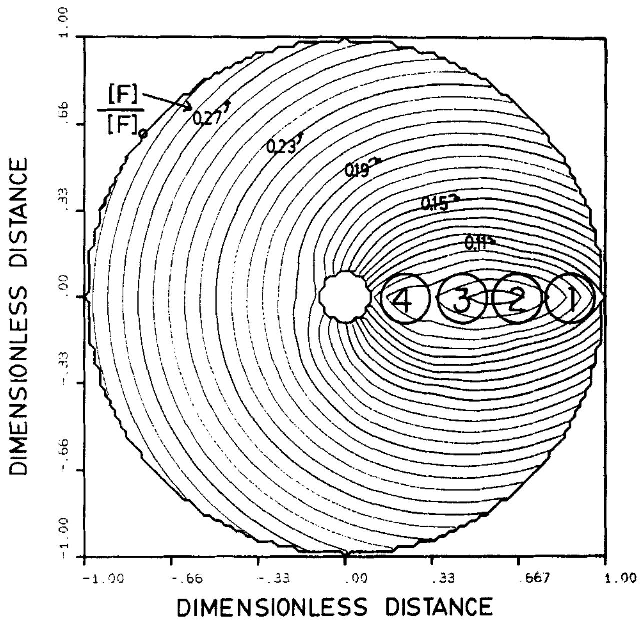

Figure 4. Contour plot of dimensionless fluorine concentration, for in-line configuration.
Reactor conditions as in Figure 3; inlet gas flow rate, 45 sccm

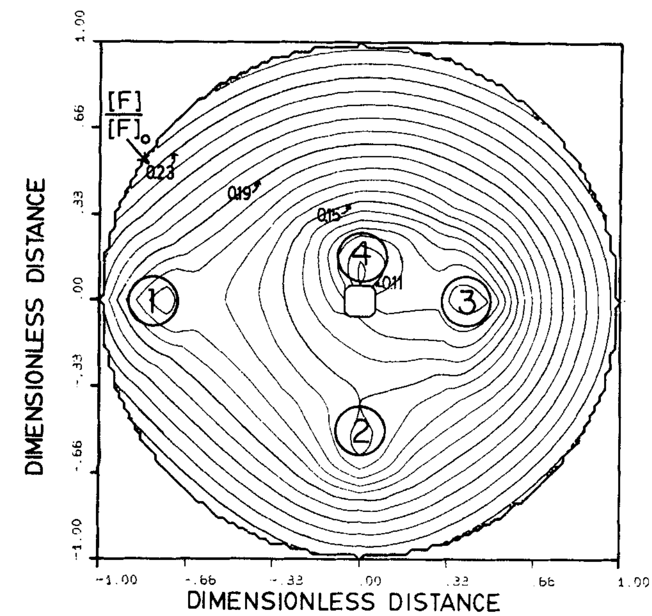

Figure 6. Contour plot of dimensionless fluorine concentration for spread-out configuration.
Reactor conditions as in Figure 5; inlet gas flow rate, 45 sccm

Figure 4 shows a map of fluorine concentration calculated from the dispersed-flow model. This contour plot clearly shows a fluorine concentration valley located over the in-line wafers. Since the silicon etch rate is first order in fluorine concentration, Eq. 5, the fluorine contour plots are proportional to etch rate where there are wafers. These contour plots not only provide wafer-to-wafer information, they also contain useful information about the etch rate profiles over individual wafers.

Figure 5 shows the results of the model prediction and the experimental results for the case of four wafers spread out in the reactor chamber. Again the model predicts the observed minimum in etch rate and closely predicts the etch rate for each individual wafer. Figure 6 is the corresponding contour plot of fluorine concentration for the spread-out case. In this plot, localized minima exist in the fluorine atom concentration (and therefore the etch rate) over each wafer. This effect, referred to as the bullseye effect, has been studied experimentally before (Nagy, 1984). However, to date no model has been derived to predict its occurrence.

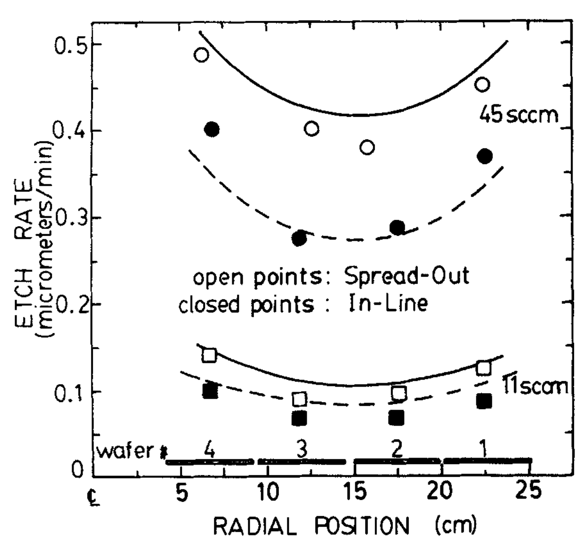

Figure 5. Predicted vs. observed wafer-averaged etch rate for spread-out vs. in-line configuration.
Temp., 25°C; press., 40 Pa; inlet NF_3 mol frac., 0.4
Model predictions: spread-out configuration, in-line configuration

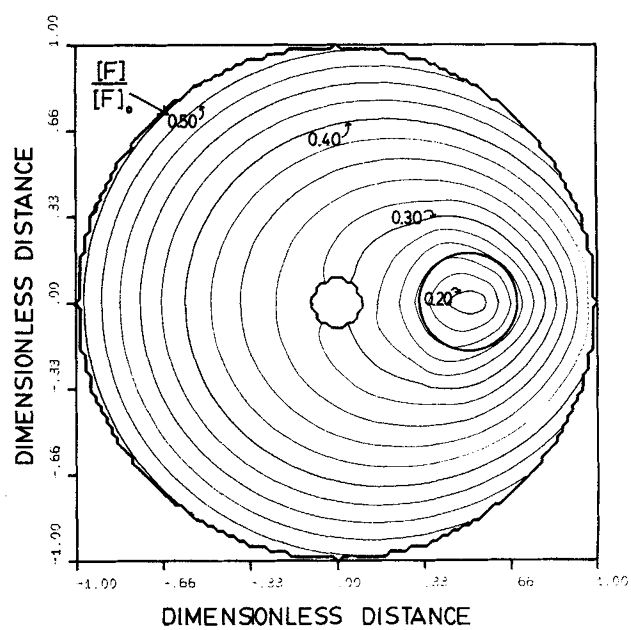

Figure 7. Whole reactor contour plot of dimensionless fluorine concentration for a single 125 mm dia. wafer.
Inlet flow rate, 100 sccm; temp., 25°C; press., 27 Pa; inlet NF_3 mol frac., 0.4

Single wafer

Although the original goal of the model was to examine interwafer nonuniformities, Figures 4 and 6 show that intrawafer information is also obtained. To examine this effect more closely, the model was solved for the case of only one wafer present in the reactor. To increase the observed effects, a wafer size of commercial interest was used (125 mm dia.). The reactor dimensions were taken from a commercial unit with an electrode diameter of 67 cm and an electrode spacing of 2.5 cm. For each single-wafer model solution, the wafer was centered at one-half the distance from the reactor center to the reactor outside radius. Although in commercial practice the reactor is more fully loaded, the single-wafer case does indicate the intrawafer nonuniformity effects obtained in an underloaded reactor.

Figure 7 plots the contours of the dimensionless fluorine concentration over the entire reactor. Since generation of fluorine atoms is extremely rapid with nitrogen trifluoride discharges (Greenberg and Verdeyen, 1985) the maximum concentration is observed at the reactor entrance (outside radius). The homogeneous loss of fluorine (from nonetching reactions) is responsible for the decrease in fluorine atom concentration in areas of the reactor where no wafer is present. Near the wafer the fluorine gradient becomes much steeper due to the etching reaction.

Figures 8a–d expand the contour plot for the single wafer solution and show the area directly over the wafer. Figure 8

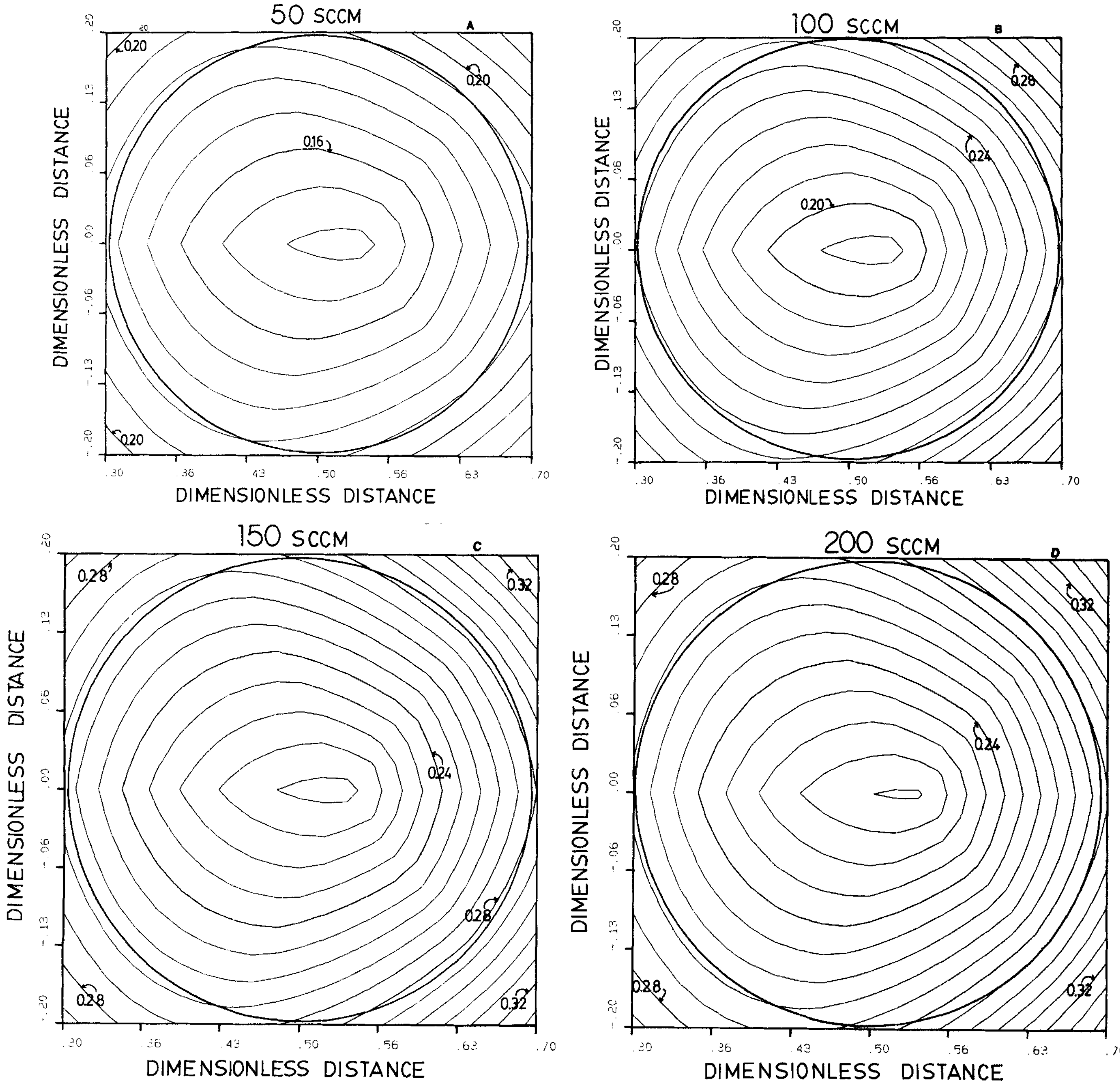

Figure 8. Contour plots of dimensionless fluorine concentration over a single 125 mm wafer.
Flow rates as indicated, other reactor conditions as in Figure 7

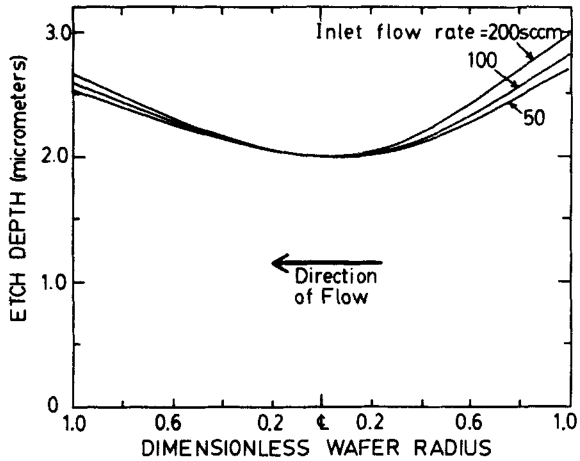

Figure 9. Single wafer etch depth plot for constant center line etch-depth of 2.0 μm.
Flow rates as indicated, other reactor conditions as in Figure 7

shows the effect of varying flow rate from 50 to 200 sccm. Although the contour plots in each case reach different fluorine atom concentration minima, the steepness of the concentration gradients are similar. To compare these variations, an etch depth calculation was made for each wafer shown in Figure 8. For this calculation, the time required to etch 2 μm (micron, micrometer) of silicon from the center of the wafer was determined using the etch rate expression given by Eq. 5. This time was then used to calculate the etch depth as a function of location over the wafer. Figure 9 plots the results of these calculations. The calculated etch times were 3.5, 3.8, and 5.1 min for 200, 100, and 50 sccm, respectively. Figure 9 illustrates that the extent of overetching incurred at the wafer perimeter is between 0.5 and 0.7 μm, or between 25 and 35% of the 2.0 μm desired etch depth. Figure 9 also shows that the overetching is only slightly dependent on flow rate, with lower flow rates giving a somewhat more uniform etch rate profile.

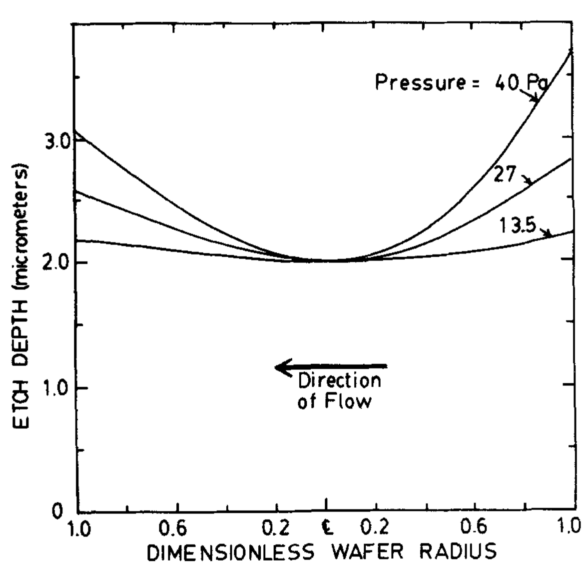

Figure 10. Single wafer etch depth plot for constant centerline etch depth of 2.0 μm.
Pressure as indicated, other reactor conditions as in Figure 7

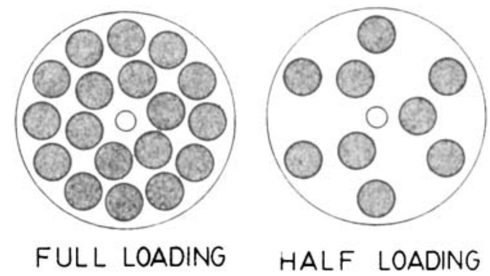

Figure 11. Commercial wafer loading configurations for 125 mm wafers in a 66 cm dia. reactor.

It is empirically known that decreasing the pressure has the effect of increasing the etch rate uniformity across a single wafer and from wafer to wafer in a single batch (Bollinger et al., 1984). This is expected since diffusion coefficients are inversely proportional to pressure. Figure 10 illustrates the effect of pressure on the uniformity of etch depth for the single-wafer case. This figure shows that a significant increase in uniformity is achieved for a factor of three change in the reactor pressure (13.5 to 40 Pa). Also evident in Figure 10 is that the upstream etch depth increases at a greater rate than does that in the downstream portion of the wafer. This is caused by the entrance flow effects increasing in importance relative to the diffusional effects.

Commercially loaded reactor

Since industrial applications normally specify larger loadings of reactors than a single wafer, the cases of a reactor loaded fully and half-loaded were modeled. Figure 11 shows the commercial wafer loading configuration for eighteen and nine 125 mm wafers in a 66 cm dia. reactor. Figure 12 plots the fluorine atom concentration contour map for the fully loaded reactor case for

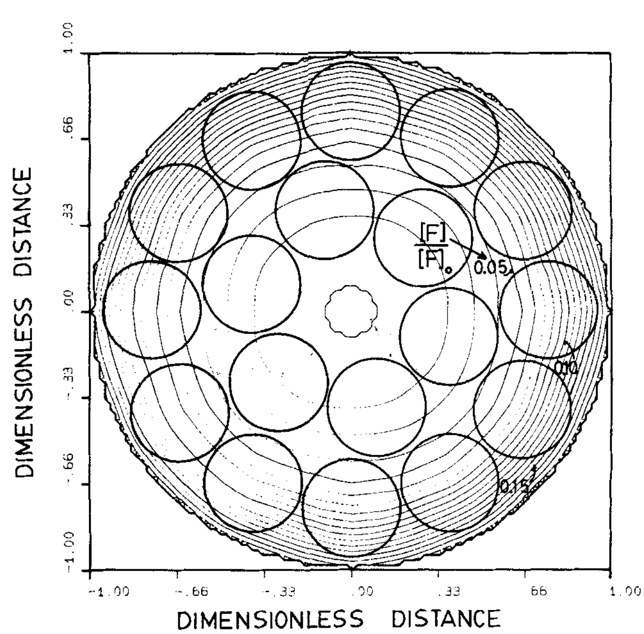

Figure 12. Contour plot of dimensionless fluorine concentration for fully loaded reactor.
Inlet flow rate, 100 sccm; temp., 25°C; press., 27 Pa; inlet NF_3 mol frac., 0.4; silicon exposed, 30%

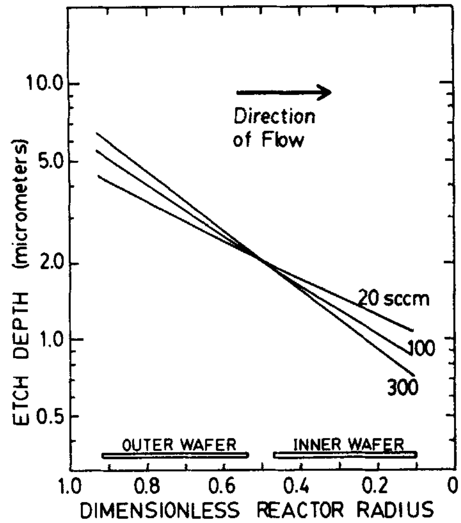

Figure 13. Effect of varying flow rate on etch depth for commercial fully loaded reactor.
Inlet flow rates as indicated; temp., 25°C; press., 27 Pa; inlet NF_3 mol frac., 0.4; silicon exposed, 30%

an inlet flow rate of 100 sccm, a pressure of 27 Pa, an inlet mode fraction of NF_3 = 0.4, and a percent silicon exposure of 30%. The percent silicon exposure accounts for the amount of silicon that would be masked by a photoresist or other nonetchable material. This contour plot shows that the presence of individual wafers is not observable in the fluorine atom patterns. To illustrate the effects of several process parameters, the etch depth at the outer and inner edge of the wafers in Figure 12 is plotted vs. reactor radial position. This etch depth is calculated for an etch depth of 2.0 μm at a dimensionless reactor radius of 0.5. Figure 13 shows that varying the inlet flow rate from 20 to 300 sccm has a slight effect decreasing the uniformity of etch rate from the inlet to outlet of the reactor. This is expected since the importance of diffusional backmixing relative to convective flow increases at low flow rates.

The importance of lower pressure on etch depth uniformity is illustrated in Figure 14. A rapid improvement in uniformity is

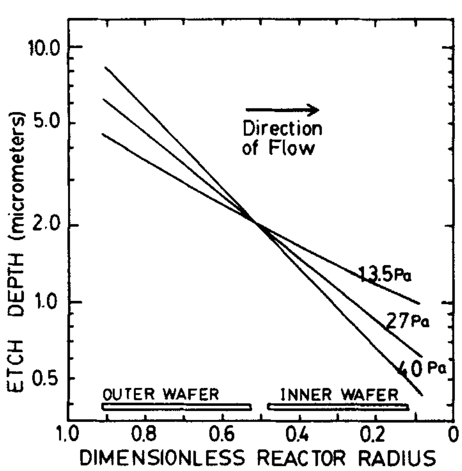

Figure 14. Effect of varying pressure on etch depth for commercial fully loaded reactor.
Pressure as indicated; 25°C; inlet flow rate, 100 sccm; inlet NF_3 mol frac., 0.4; silicon exposed, 30%

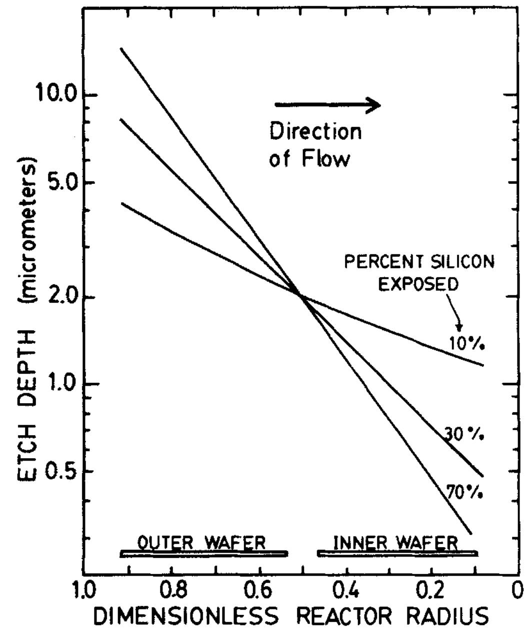

Figure 15. Effect of varying percent silicon exposed on etch depth for commercial fully loaded reactor.
Percent silicon exposed as indicated; temp., 25°C; press., 27 Pa; inlet NF_3 mol frac., 0.4; inlet flow rate, 100 sccm

achieved as the pressure is decreased from 40 to 13.5 Pa. This improvement is due to increased diffusional backmixing, combined with the lower etch rates at lower pressures (i.e., lower concentrations of fluorine atoms), resulting in lower conversions. Thus the reactor approaches the case of a differential reactor. The final parameter examined is the percent silicon exposed. Figure 15 shows that decreasing the silicon exposure on

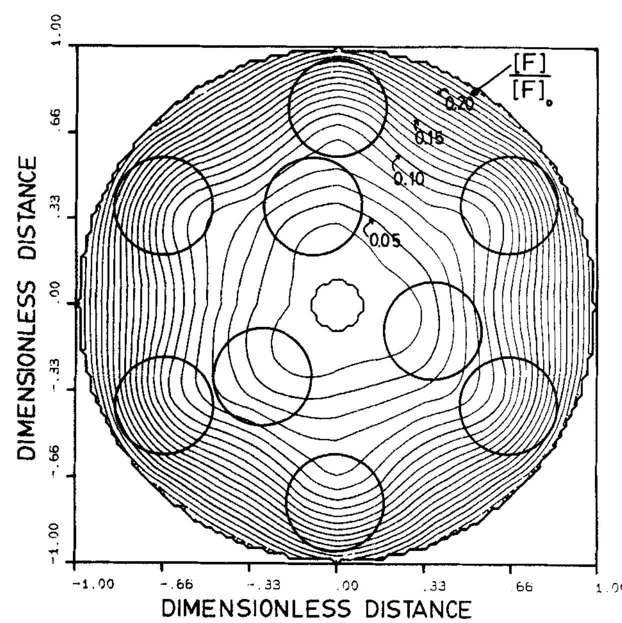

Figure 16. Contour plot of dimensionless fluorine concentration for half-loaded reactor.
Inlet flow rate, 100 sccm; temp., 25°C; press., 27 Pa; inlet NF_3 mol frac., 0.4; silicon exposed, 30%

the 125 mm wafers rapidly increases the uniformity of the etch depth from the inlet of the reactor to the outlet. As in the case of lowering pressure, lowering the amount of etchable material decreases the fluorine conversion and thus the reactor approaches differential conditions.

Since the commercial fully loaded reactor did not result in significant etch rate gradients in the tangential direction, the case of a half-loaded reactor, Figure 11, was investigated. Figure 16 shows the results of the model for this case. Unlike the fully loaded reactor, the loction of the wafers is observable in the fluorine concentration contours. Therefore some variation in the etch rate is expected in the θ direction for the half-loaded case.

Summary and Conclusions

Etch rates of silicon wafers in a plasma discharge of nitrogen trifluoride were measured as a function of wafer location in a radial flow reactor. Variations in flow rate, pressure, percent silicon exposed (etchable wafer area), reactor loading, and wafer positioning were investigated.

A discrete partial differential model was written and solved using finite elements to predict the etch rate based on previously measured reaction rate parameters (Stenger and Akiki, 1986). To include the effects of the low operating pressures in plasma etching (<60 Pa), flow by diffusion was included, which resulted in a linear second-order partial differential equation subject to the Danckwerts boundary conditions. The solution was complicated by the discrete nature of the silicon wafers. Since the reactor was not uniformly covered by silicon, the model was solved with an etch rate term in the presence of silicon, and without the etch rate term in locations of the reactor where there was no silicon.

The model successfully predicted the etch rate of silicon within accuracies of 5% for wafers located in various patterns within the reactor and inlet gas flow rates between 11 and 59 standard cubic centimeters per minute. It was also able to predict the experimentally observed existence and location of a minimum in the etch rate between the inside and outside reactor radius.

The accuracy of this model is only confirmed within the range of conditions where our experimental data have been taken. It is expected that the model's predictive capability will extend outside this range within limits, but may lose its accuracy at very different pressures, flow rates, and applied powers. However, the use of the model outside the range of our data will identify important parametric trends. Therefore the model was extended to evaluate the intrawafer nonuniformities in etch depth for a reactor with either single or multiple wafers being etched, as is commercially done. In all cases more uniform etching was achieved by reducing the pressure and the etchable fraction of the wafer surface. A marginal improvement was obtained by reducing the flow rate.

Notation

a_{Si} = exposed silicon area per volume of reactor
a = dimensionless averaged radial bulk velocity at outside radius of reactor boundary
b = dimensionless loss reaction rate constant
B_i = Biot number
c = dimensionless etching rate constant
c_a = concentration of fluorine atoms in reactor
$\bar{c}$ = averaged concentration of fluorine atoms in reactor
$\bar{c}_0$ = averaged concentration of fluorine atoms at outside radius of reactor boundary
$\mathcal{D}$ = diffusivity of fluorine atoms in argon
h = half the total electrode spacing
k_1 = dissociation rate constant
k_2 = etching rate constant
k_3 = loss reaction rate constant
r = radial coordinate
r_F = rate of disappearance from gas phase of F
r_{NF_3} = rate of disappearance from gas phase of NF_3
r_{Si} = rate of disappearance from gas phase of Si
r_{SiF_4} = rate of disappearance from gas phase of SiF
r_i = inside radius of reactor boundary
r_o = outside radius of reactor boundary
$S(r,\theta)$ = step function, =1 only over wafer surface
v_r = radial bulk velocity
$\bar{v}_r$ = averaged radial bulk velocity
v_z = axial bulk velocity
v_θ = tangential bulk velocity
$\bar{v}_o$ = averaged radial bulk velocity at outside radius of reactor boundary
x = stoichiometric coefficient of dissociation reaction, Eq. 1
x = radial coordinate
x_i = inside radius of reactor boundary
y = averaged concentration
z = axial coordinate
θ = tangential coordinate

Literature cited

Alkire, R. C., and D. J. Economou, "Transient Behavior During Film Removal in Diffusion-Controlled Plasma Etching," *J. Electrochem. Soc.*, **132**(3), 648 (1985).
Battey, J. F., "The Effects of Geometry on Diffusion-Controlled Chemical Reaction Rates in a Plasma," *J. Electrochem. Soc.*, **124**(3), 437 (1977).
Bird, R. B., W. E. Stewart, and E. N. Lightfoot, *Transport Phenomena*, Wiley, New York, 505 (1960).
Bollinger, D., S. Iida, and O. Matsumoto, "Reactive Ion Etching: Its Basis and Future," *Solid State Technol.*, **27**(6), 167 (1984).
Bower, D. H., "Planar Plasma Etching of Polysilicon Using CCl_4 and NF_3," *J. Electrochem. Soc.*, **129**(4), 795 (1982).
Chow, T. P., and A. J. Steckl, "Plasma Etching of Refractory Gates for VISI Applications," *J. Electrom. Soc.*, **131**(10), 2325 (1984).
Eisele, K. M., "SF_6, a Preferable Etchant for Plasma Etching Silicon," *J. Electrochem. Soc.*, **128**(1), 123 (1981).
Ephrath, L. M., "Selective Etching of SiO_2 Using Reactive Ion Etching with CF_4/H_2," *J. Electrochem. Soc.*, **126**(6), 1419 (1979).
Flamm, D. L., "Measurements and Mechanisms of Etchant Production During the Plasma Oxidation of CF_4 and C_2F_6," *Solid State Technol.*, **22**(4), 10, (1979).
Flamm, D. L., V. M. Donnelly, and J. A. Mucha, "The Reaction of Fluorine Atoms with Silicon," *J. Appl. Phys.*, **52**(5), 3633 (1981).
Flamm, D. L., V. M. Donnelly, and D. E. Ibbotson, "Basic Principles of Plasma Etching," *VLSI Electronics, Microstructure Science*, Academic Press, New York (1984).
Fonash, S. J., "Advances in Dry Etching Processes—A Review," *Solid State Technol.* **28**(1), 150 (1985).
Greenberg, K. E., and J. T. Verdeyen, "Kinetic Processes of NF_3 Etchant Gas Discharges," *J. Appl. Phys.*, **57**(5), 1596 (1985).
Hess, D. W., "Plasma Etch Chemistry of Aluminum and Aluminum Alloy Films," *Plasma Chem. Plasma Process.*, **2**(2), 141 (1982).
Honda, T., and W. W. Brandt, "Mass Spectrometric Transient Study of DC Plasma Etching of Si in NF_3 and NF_3/O_2 Mixtures," *J. Electrochem. Soc.*, **131**(11), 2667 (1984).
Ianno, N. J., K. E. Greenberg, and J. T. Verdeyen, *J. Electrochem. Soc.*, **128**(9), 2174 (1981).
IMSL, "TWODEPEP," International Mathematical and Statistical Libraries, Houston (1983).
Jensen, K. F., M. Dalvie, and D. B. Graves, "Modeling of Reactors for Plasma Processing. I: Silicon Etching by CF_4 in a Radial Flow Reactor," *Chem. Eng. Sci.*, **41**(4), 653 (1986).
Korman, C. S., T. P. Chow, and D. H. Bower, "Etching Characteristics of Polysilicon, SiO_2, and $MoSi_2$ in NF_3 and SF_6 Plasmas," *Solid State Technol.*, **26**(1), 115 (1983).
Mathad, G. S., "Review of Single Wafer Reactor Technology for Device Processing," *Solid State Technol.*, **28**(4), 221 (1985).

Mogab, C. J., "The Loading Effect in Plasma Etching," *J. Electrochem. Soc.*, **124**(8), 1262 (1977).
———, "Dry Etching," *VLSI Technology*, S. M. Sze, ed., McGraw-Hill, New York, ch. 9 (1984).
Mogab, C. J., A. C. Adams, and D. L. Flamm, "Plasma Etching of Si and SiO_2—The Effect of Oxygen Additions to CF_4 Plasmas," *J. Appl. Phys.*, **49**(7), 3796 (1978).
Nagy, A. G., "Radial Etch Rate Nonuniformity in Reactive Ion Etching," *J. Electrochem. Soc.*, **131**(8), 1871 (1984).
Sawin, H. H., "A Review of Plasma Processing Fundamentals," *Solid State Technol.*, **28**(4), 211 (1985).
Sawin, H. H., and B. Thompson, "Continuum Modeling of Charged Particle Transport in RF Breakdown and Discharges of SF_6," *Mat. Res. Soc. Symp. Proc.*, Spring Meeting, 68, (1986).
Stenger, H. G., Jr., and G. S. Akiki, "Kinetics of Plasma Etching Silicon with Nitrogen Trifluoride," *Mat. Res. Soc. Symp. Proc.*, **68**, 267 (1986).
Tokunaga, K., and D. W. Hess, "Aluminum Etching in Carbon Tetrachloride Plasmas," *J. Electrochem. Soc.*, **127**(4), 928 (1980).
Winters, H. F., J. W. Coburn, and E. Kay, "Plasma Etching—A Pseudo-Black-Box Approach," *J. Appl. Phys.*, **48**(12), 4973 (1977).
Woytek, A. J., J. T. Lileck and J. A. Barkanic, "Nitrogen Trifluoride—A New Dry Etchant Gas," *Solid State Technol.*, **27**(3), 172 (1984).
Zarowin, C. B., "Relation between the RF Discharge Parameters and Plasma Etch Rates, Selectivity, and Anisotropy," *J. Vac. Sci. Technol. A*, **2**(4), 1537 (1984).
———, "A Theory of Plasma-Assisted Chemical Vapor Transport Processes," *J. Appl. Phys.*, **57**(3), 929 (1985).

Manuscript received Nov. 24, 1986, and revision received Feb. 9, 1987.